Mass Transfer across the Turbulent Gas–Water Interface

Z. F. Xu and B. C. Khoo
Dept. of Mechanical Engineering, National University of Singapore, Singapore 119260

K. Carpenter
Institute of Chemical and Engineering Sciences, Singapore 627833

DOI 10.1002/aic.10972
Published online August 30, 2006 in Wiley InterScience (www.interscience.wiley.com).

Mass transfer across the gas–water interface is important in many fields, but the present understanding of the scalar transport as mediated by the complex near-surface turbulence is still far from complete. In this work, an innovative particle image velocimetry (PIV)–based measurement method was used to investigate the near surface turbulence. Turbulence measurement with respect to the fluctuating interface was performed and the gradient of the vertical fluctuating velocity (Hanratty's β) deemed as a critical controlling parameter was quantified. Several distinctly different but typical flow conditions were investigated and the associated mass-transfer velocity was measured. Based on these experimental works, an empirical relation, very similar to that proposed earlier by Law and Khoo, relating the mass transport across the turbulent interface to the turbulence parameter β, was determined in the midst of vastly different flow conditions where turbulence is induced simultaneously from above and beneath the gas–water interface. © 2006 American Institute of Chemical Engineers *AIChE J,* 52: 3363–3374, 2006
Keywords: mass transfer, gas–water interface, Hanratty's β, linear region, PIV

Introduction

Scalar transport across the turbulent gas–water interface has enormous importance in various natural and man-made industrial processes. Because of its wide application, a general model capable of predicting the scalar (heat or mass) transfer velocity across the gas–water interface is highly desirable and remains the objective of many researchers. The interfacial mass transfer is, by its very nature, highly complex: the gas and the water may be in a state of turbulent motion, and the interface is highly irregular, and possibly accompanied by waves with and without wave breaking and the associated entrainment and formation of bubbles.

For sparingly soluble gases, the diffusivity in the gaseous phase is usually much greater than that in water. Thus the gas-side dynamics are less critical and the transport is determined predominantly by the water-side hydrodynamics. Mass transfer of gases through the gas–water interface is affected by many factors, such as the difference of concentration between the phases, temperature, flow conditions, and even more so the conditions or state of turbulence motion right at the interface where the expected concentration boundary layer is embedded (for example, see Law and Khoo,[1] in their work relating the mass transport across the turbulent interface). Molder et al.,[2] Vasconcelos et al.,[3] and McKenna and McGillis[4] did further analysis on the effect of the presence of surfactants and insoluble compounds on the interface. It is surmised that the surfactants/contaminations can physically interfere with the transfer process or dampen and reduce the turbulent motion in the vicinity of the interface.

In the absence of the above-mentioned surface-seeking contaminations and surfactants, the state of turbulent motion in the vicinity of the interface where the concentration boundary is embedded is deemed to be the dominant factor affecting the transport rate across the interface. To correlate the mass-trans-

fer velocity with suitable hydrodynamics parameters reflecting the turbulence conditions, many theories have been proposed to describe the mechanism governing the gas–water mass transfer. Theofanous,[5] in a review of various conceptual models, identified these different models into two major classes: (1) the eddy diffusivity model and (2) the eddy structure model. In the eddy diffusivity model, a relation between the mass-transfer velocity K_L, the diffusion coefficient D, and the thickness of the diffusion film δ is proposed as

$$K_L = \frac{D}{\delta}. \tag{1}$$

As such, the thickness of the diffusion film δ is selected to characterize the hydrodynamics near the interface. The other class is the eddy structure model. It is also known as "surface renewal" model. The model is expressed in the following form:

$$K_L = \sqrt{\frac{D}{\tau}}. \tag{2}$$

The averaged surface renewal time (τ) is thought to govern the mass transfer across the water interface. The difficulty with these conceptual models is that somehow the selected parameters (δ or τ) must still be reasonably easy to characterize and make related to the near-interface turbulence controlling the mass transfer. As Tamburrino and Gulliver[6] indicated, the measurements of "surface renewal eddies" are difficult to correlate with the mass-transfer velocity because the investigators themselves have to define what constitutes a surface renewal eddy.

Until now, there has been no broad consensus with respect to a general and yet sufficiently robust model that is capable of predicting the transfer velocity under different flow conditions. Most models are based on parameters that are directly dependent on the particular means of turbulence generation and/or experimental setups and geometries. Such models may not be applicable under other turbulence conditions. Fundamentally, the exchange of gases across the gas–water interface occurs across a thin boundary layer at the gas–water interface. The details of the boundary layer are determined by the hydrodynamics near the surface. A robust model should be based primarily on the hydrodynamic parameters obtained directly from the turbulence structure in the very vicinity of the interface.

In a review of various works, Hanratty[7] highlighted the development of a model that relates the mass-transfer velocity directly to the hydrodynamics near the interface without resorting directly to the above-mentioned conceptual models. Because the concentration boundary layer is very thin, the derivative in the normal direction (z-) is much larger than in the other directions. Therefore, using a coordinate system embedded on the interface, the boundary-layer equation for concentration (C) in a turbulent flow field near a free surface can be simplified as

$$\frac{\partial C}{\partial t} + w\frac{\partial C}{\partial z} = D\frac{\partial^2 C}{\partial z^2}. \tag{3}$$

McCready et al.[8] conducted a series expansion and order-of-magnitude analysis near the interface and deduced the following relation for the vertical velocity:

$$w = \beta z. \tag{4}$$

That is, at the vicinity of the interface, w varies linearly with z with a gradient of β. From Eqs. 3 and 4, the importance of β is apparent to mass transfer across the gas–water interface.

The interest in β as the crucial parameter governing the interface mass transfer provided the motivation for the development of a technique that can simultaneously measure the undulating interface and the flow field just beneath it. Particle image velocimetry (PIV)–based technique provides an advantage of noninterference of the flow field and facilitates measurements of the whole flow field at that same time to be carried out. Hassan et al.,[9] Peirson,[10] Law et al.,[11] and several other researchers proposed some techniques based on the PIV technique, with the intention of measuring the interface fluctuation as well as the velocity just beneath it. Based on the measurement technique of Law et al.,[11] Law and Khoo[1] carried out a series of experimental works with two vastly different flow conditions and found that the selected near-surface turbulence parameter (β) provides a reasonable model for interfacial mass transfer. Their relation is expressed as

$$K_L^+ \mathrm{Sc}^{0.5} = 0.22(\beta_{rms}^+)^{0.5}. \tag{5}$$

This is perhaps the first time a correlation was presented to account for two very different means of turbulence generations: one from above in the gaseous phase and the other from beneath the interface in the water.

It is noted that these two different turbulence generation means were carried out separately: either from above or below, but not simultaneously. The validity and accuracy of the model is also not tested more extensively. In this work, it is our intent to improve on the measurement technique of Law and Khoo,[1] and conduct a series of experiments with more varied flow conditions. In particular, the critical parameter β was measured for several representative flow arrangements encountered in the environment: turbulence generated from above (in the gaseous phase) as in wind-induced flow, turbulence generated simultaneously from above and below in the same direction, and simultaneously generated in the opposite direction. In the midst of such measurements, the mass-transfer experiment was carried out with the aim of providing a relationship between the mass-transfer velocity and the selected hydrodynamics parameter β for comparison with Law and Khoo.[1] In this work, oxygen is intentionally introduced and used as the tracer gas instead of carbon dioxide as in Law and Khoo,[1] and a more general correlation is anticipated.

Experimental Setups

The experiment was carried out in a circular wind-wave channel tank with two water jet streams directed in the tangential streamwise direction at the bottom. Figure 1 shows the schematic diagram of the circular water tank.

The apparatus consisted of an annular water channel with 10-cm depth, 10-cm width, with 40-cm ID and enclosed in a

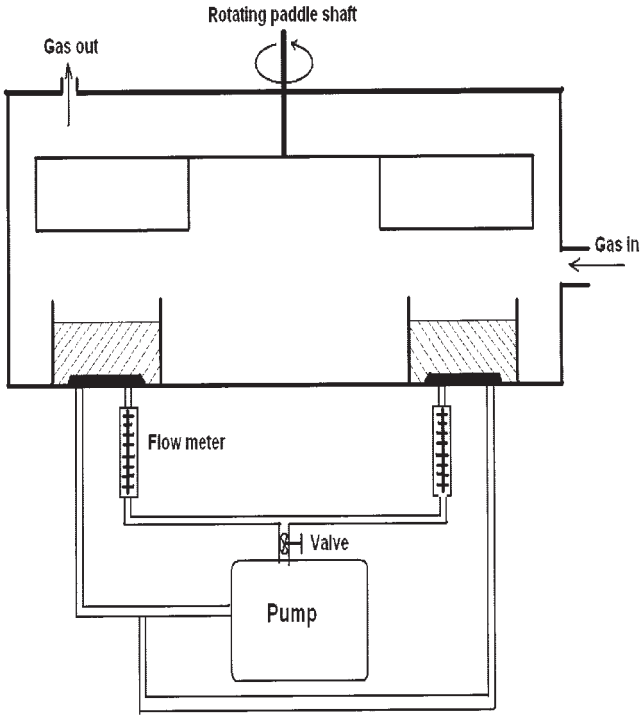

Figure 1. Circular water tank (not to scale).

75-cm diameter external cylindrical tank. The entire setup was made of transparent Perspex material, so as to facilitate flow visualization and measurement. The wind was generated by means of a rotor with four Perspex paddles (20 cm width) arranged at right angles above the annular channel. The distance between the paddles and the water surface can be adjusted, and the rotating speed and rotating direction of the paddles were controlled by a rotor. The two water jet streams through four 3-mm diameter nozzles (placed diametrically opposite) beneath the interface can generate a clockwise direction streamwise flow directed along the bottom of the circular tank by the inlets and outlets connected to a water pump. The speed of the water jet generated can be varied using a ball valve and the volumetric flow rate was measured with a flow meter. So by using these two independent means of turbulence generation from above and beneath the gas–water interface, we can achieve a variety of flow conditions imposed on the water surface and its vicinity. In this work, several representative kinds of flow conditions were chosen. These were generated by solely wind shear from above and the simultaneous generation by wind shear from above and water jet from beneath in the same and opposite directions. These representations of turbulence generation are deemed more general and perhaps all encompassing. They can be considered as a reasonable simplification of most real-life complex flow conditions.

In the experiments, fresh tap water was filled to a depth of 7.5 cm in the channel and the paddles were located at about 7.5 cm above the water surface. The flow rate through the water pump was adjusted with the combination of a ball valve and a flow meter. With a given flow rate from beneath, the turbulence intensity near the interface is still a function of the variable imposed wind speed. Table 1 summarizes the groups of different flow conditions studied.

For purpose of reference, the notional gas flow speed above the water surface is assumed to be the same as the paddle speed, which is taken directly above the center of the 10-cm width water channel. This method of referencing follows that of Law et al.,[11] where

$$V_{wind} \approx R\omega. \tag{6}$$

Here ω is the rotation speed of the rotor driving the paddles and R is the distance from the center of the rotation shaft to the center of the water channel. The rotation speed of the rotor was measured using a tachometer. The paddle speed above the center of the water channel is taken as the parameter denoting the quality of turbulence generated at the water surface of the wind wave channel. Because the major or practically all of the resistance to the mass transfer in this experiment (low solubility gas is used) resides in the water side, accurate measurement of the wind velocity profile in the vicinity of the interface is deemed unnecessary and will not aid further in the quantification of the critical parameter influencing the interfacial mass transfer.

The range of nominal wind speeds carried out in this study is 3.00 to 7.00 m/s. The upper limit wind speed is chosen such that the turbulence intensity generated is well below the limit where wave breaking occurs.

For these experiments, the circular wind-wave channel is sealed by a gastight lid. The tracer gas is input through the opening at the side of the tank, and residual gas is exhausted out of the system through the outlet opening located at the top.

Technique for measuring near-surface turbulence

The presence of a meniscus at the point of contact between the water and channel wall can cause some difficulties/uncertainties in visualizing the flow field at the vicinity of the interface. In the early PIV-based experiments (such as the works of Jahne and Wierzimok[12] and Hassan et al.[9]), the difficulties lie in accurately determining the interface position without affecting the near-surface flow conditions. Another class of method was based on the optical property of laser light,

Table 1. Summary of the PIV Experimental Conditions

Flow Condition	Flow Rate (mL/s)	Direction	Nominal Wind Speed (m/s)
Case 1	0		3, 3.5, 4, 4.5, 5, 5.5, 6, 6.5, 7
Case 2	6.3	Opposite	3, 3.5, 4, 4.5, 5, 5.5, 6, 6.5, 7
Case 3	6.3	Same	3, 3.5, 4, 4.5, 5, 5.5, 6, 6.5, 7
Case 4	3.2	Opposite	3.5, 4.5, 6, 6.5
Case 5	3.2	Same	3.5, 4.5, 6, 6.5
Case 6	10.5	Opposite	3.5, 4.5, 6, 6.5
Case 7	10.5	Same	3, 3.5, 4.5, 6, 6.5

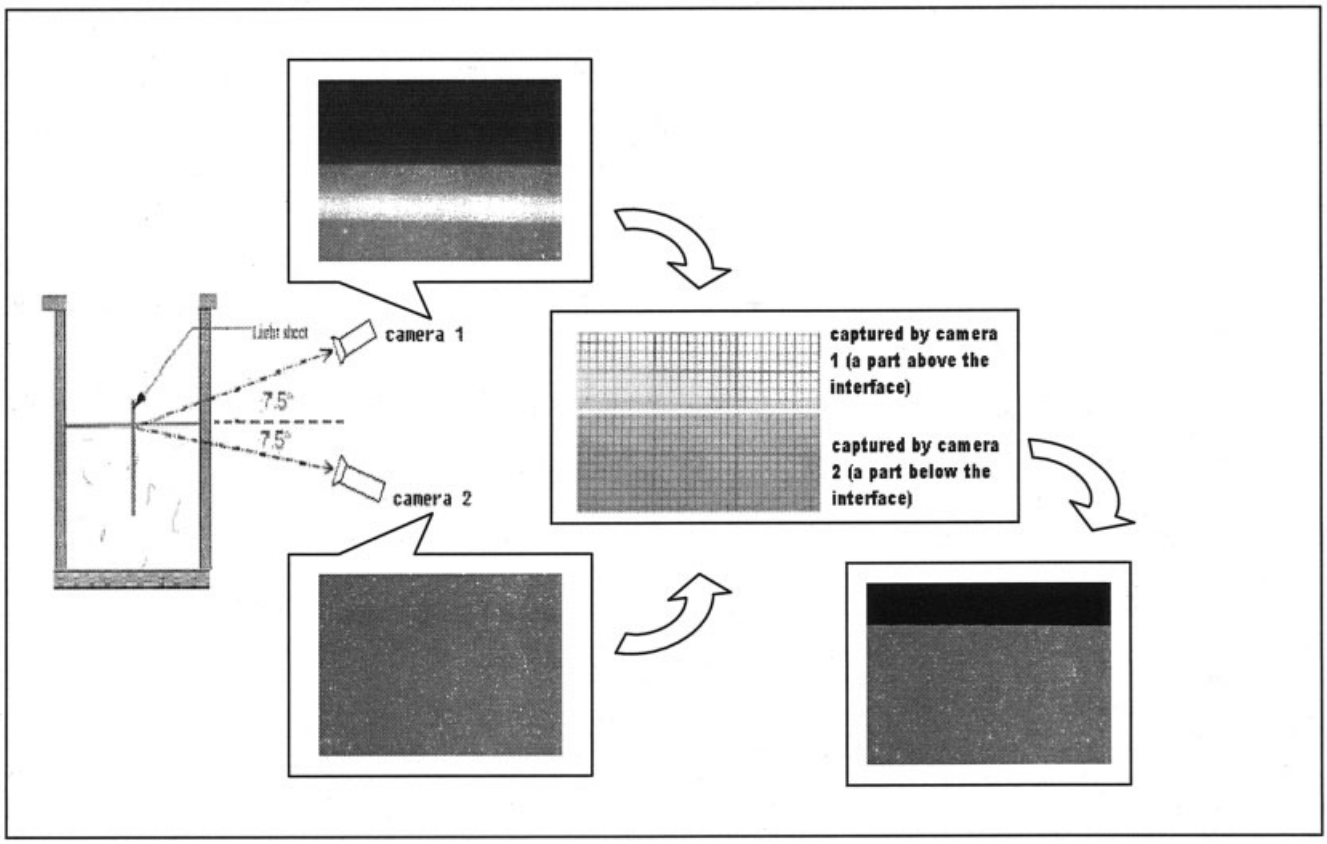

Figure 2. Observing angles and interface detection.

of which representative works include Lorencez et al.,[13] Baumann et al.,[14] and Lin and Perlin.[15] This method, although capable of determining the interface position without affecting the near-surface flow conditions, did not allow or facilitate the simultaneous measurement of the flow field above and beneath the gas–water interface.

To avoid the meniscus effect, Munsterer and Jahne[16] suggested observing the interface and the flow field beneath it from a position slightly below the water surface. Peirson[10] used a camera to observe and determine the interface wave motion from above, thus producing an unobstructed and good visualization of the interface. Inspired by these two mentioned works, Law et al.[11] implemented two pairs of viewing mirrors to reflect the two different views onto a single plane.

In the present work, with the availability of two independent camera systems, further improvements can be made for a more accurate quantification of the interface position and improvement of the spatial resolution of the flow field close to the interface.

Figure 2 shows the schematic diagram for arrangement of the two titled cameras (PixelFly HiRes® model). Camera 1 and camera 2 were adjusted separately and tilted at a small angle of about 7.5° to the horizontal. These small angles, obtained after numerous trials, ensure unobstructed and clear visualization of the flow field for all of the imposed flow conditions, while keeping the magnification difference between the top and bottom (known as distortion) not exceeding 5%. To visualize the water surface as a continuous edge, fluorescent dye was introduced to illuminate the visualization plane, which is similar to the work of Law et al.[11]

The typical images captured simultaneously from camera 1 and camera 2 are also shown in Figure 2. With the introduction of fluorescent dye, the water side glows with certain luminance intensity, different from that of the particles. The interface is located at the edge of the contrast between the fluid and the gas. The advantage of using fluorescent dye to visualize the interface is that, regardless of the interface fluctuation, the interface will always be visualized as a continuous edge of luminance contrast. The dye also produces contrasting luminance intensity from the particle seedings to allow use of the PIV technique.

Before the start of an experiment, a careful scaling calibration step is needed to correlate the images captured by camera 1 and camera 2. A referenced scale is set to "puncture" the water surface at the plane of observation (coincide with the laser sheet plane). Images are captured by each camera and compared pixel by pixel. After obtaining the interface location from camera 1, a program is written to "transform" the interface location to the bottom view (camera 2) using the bottom view local scaling. The program is used to scale and correlate the images so that both the horizontal and vertical alignments are achieved. Some parts of the referenced scale images captured by the two cameras and the "transforming process" from camera 1 to camera 2 are also shown in Figure 2.

The conventional edge-detection technique is based on finding the "maximum gradient" point. Given that the particles ($\sim$20 μm PSP) are brighter than water, edge detection working

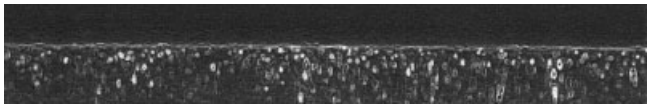

Figure 3. Edge detection worked on the near surface region (gray image).

directly on the gray images of the gas–water interface (captured from camera 1) will simultaneously reveal the edge of particles and the interface (see Figure 3). To filter out the particle points seeded in the water side, an optimal threshold value of intensity is chosen to carry out a binary operation. Taking account of the possible uneven distribution of light intensity along the interface, the interface region is divided into a subset of discretized surface regions and the binary operation is performed in each small part. The threshold level is determined by analyzing the histogram of the corresponding small part. A Matlab (The MathWorks, Natick, MA) program is written to perform all of these operations based on the technique described by Rider and Calvard.[17] After the binary operation, edge detection can then be used to determine the interface location. Figure 4 shows the interface profile detected by this method. It is shown to be accurate by comparison with the original image and the uncertainty is controlled within ± 1 pixel. Figures 3 and 4 show just the region near the interface.

Compared to the work of Law et al.,[11] the present use of two independent camera systems helps to overcome the abovementioned two difficulties brought in by trying to capture the two distinct views onto a single imaging plane. In addition, these two independent cameras provide a much higher resolution (about 20 μm/pixel). These improvements ensure a clearer visualization of the interface and the associated flow field in the water side. The interface position can be determined more accurately. Because the image resolution is the major source of measurement uncertainty, the present higher resolution has improved the experimental accuracy.

Analysis for the flow field beneath the water surface is performed using a commercial PIV software (FlowManager). An adaptive correlation technique was adopted to calculate the velocity profile of the flow field because it can provide an increased dynamic range and accuracy. Following Law et al.,[11] the velocity with respect to the interface can be deduced by taking the difference between the velocity (v) and the interface velocity located directly above the interrogation area of the velocity vector (v_i):

$$v_r(z) = v(z) - v_i. \tag{7}$$

To obtain the variation of vertical rms velocity with depth, many image pairs (36 pairs in this work) have to be analyzed and the vertical rms velocity is calculated by ensemble averaging of velocity located at similar depth from the interface. Precision uncertainty is reduced to about 2% by the ensemble average operation. Other details on the measurement of the flow field and interface velocities can be found in Law et al.[11] and thus are not repeated here.

Technique for measuring the interfacial mass-transfer velocity

In this work, mass-transfer velocity is determined by measuring the dissolved oxygen evasion rate and absorption rate. Gas-exchange velocities are determined by a disturbed equilibrium method. The water concentration of the dissolved oxygen to be measured is perturbed from equilibrium before an experiment and the gas-transfer velocity is computed by measuring the rate of return to equilibrium. The time rate of change in the tank of water is given by

$$\frac{dC}{dt} = K_L A(C_s - C)/V_w \tag{8}$$

where V_w is the volume of water in the test system, A is the nominal area of the interface without waves, C is the bulk concentration of dissolved oxygen in water, C_s is the saturation concentration of oxygen at the interface, and K_L is the bulk liquid-side mass-transfer coefficient. The solution to Eq. 8 is as follows:

$$K_L = \left(\frac{V_w}{At_f}\right) \ln \frac{(C_s - C_i)}{(C_s - C_f)} \tag{9}$$

where C_i is the initial concentration of gas in the bulk water and C_f is the final concentration after time t_f.

The mass-transfer velocity measurements were carried out separately from the turbulence measurements, and it is noted that precaution were taken to clean the interface well before each experiment, as discussed at length in Law and Khoo[1] and not repeated here. Because the tracer gas is stored at a temperature cooler than the bulk water in the test section, it needs to be preheated to the same temperature before being introduced into the setup. This is done by passing the gas through a heat exchanger, immersed in a large water bath. The water temperature in the test section is monitored with a thermometer to ensure that the variation is below ± 0.5°C. In the test section, the tracer gas is introduced just above the interface and with special care taken so as not to induce any interface disturbance. Before each experiment, the tracer gas is introduced for at least 20 min (for evasion experiments) or 10 min (for absorption experiments) to ensure a uniform initial condition. The most important aim is to prevent any buildup of noncondensable gases (notably air) residing close to the interface.

For the gas evasion experiments, CO_2 was used to continually flush the tank headspace to yield a known zero oxygen surface concentration (that is, $C_s(t) \approx 0$ mg/L). For the gas absorption experiments, pure O_2 was introduced such that the total gaseous volume above the interface was considered to be saturated. Under such condition, C_s is maintained at the water surface at water temperature; this value can be obtained from the manual supplied by the sensor manufacturer (in agreement with published measurements).

By measuring C_i and C_f, the water-side mass-transfer velocity K_L can be determined. In this work, bulk water-side dissolved oxygen concentration was measured using a commercial

Figure 4. Edge detection worked on the near surface region (binary image).

fiber-optic oxygen sensor (model 210, Instech Laboratories) with an accuracy of 1%. The sensor uses two standards of known oxygen concentration and a linear algorithm for calibration. In this work, the two known oxygen concentration standards are zero concentration standard and atmospheric saturated concentration standard. The zero standards are obtained by adding sodium sulfite to DI (deionized) water. To prepare the atmospheric saturated standards, starting with DI water from a bottle held at ambient temperature for an extended period of time, and transferring it from cup to cup with ample turbulence at least 20 times. This procedure followed the instruction of DQM standard operation procedure (Katzenlson[18]). According to the theory of operation, the sensor will be most sensitive to low levels of oxygen and deviations from the linear relation occur primarily at higher oxygen concentration levels. The working range for oxygen evasion experiment was within the calibration range, whereas the absorption experiment was conducted in the extrapolated range of calibration. A shorter time interval was therefore adopted to obtain the final water samples in the gas absorption experiment, which helps to ensure that the working range in the absorption experiment is not far away from the linear calibration range, although it may be mentioned that the gas absorption experiment is still less accurate than the gas evasion experiment. Nevertheless these two means were used as a self-consistent check and to demonstrate that essentially the correlation relationship obtained is independent of the direction of scalar transport.

Concentrations of C_i and C_f were obtained as the average values of at least five samples with a variation $< 2\%$. Taking into account the measurement uncertainty introduced by the instrument calibration, the overall measurement uncertainty for the gas evasion experiment is estimated to be $<5\%$. On the other hand, the measurement uncertainty for the gas absorption experiment is estimated to be about 10% or higher and attributed to the limitation posed by the oxygen probe.

Data Analysis and Results

Near-surface vertical velocity gradient

Figure 5 shows the typical variation of the vertical fluctuating velocity with respect to the interface (for Case 3 with nominal wind speed = 5 m/s). It can be seen that the vertical fluctuating velocity measured with respect to the interface increases with depth. This quantity tends toward zero as the interface is approached.

It can be seen from Figure 5 that a linear region appears to exist near the interface. This is in agreement with the analysis of McCready et al.[8] and confirmed in the experiments of Law and Khoo.[1] A linear fit through the origin was performed on the data points located at the immediate vicinity of the interface to provide a coefficient of determination (R^2 coefficient) still >0.85 for all experiments.

The most important parameter β_{rms} is defined as the gradient of the $V_{r\text{-rms}}$ profile near the interface, which can be deduced from Eqs. 3 and 4 to relate to the mass transfer across the turbulent gas–water interface. Together with the gradient of the linear variation, two other parameters can be obtained to characterize the near-surface turbulence conditions as carried out in Law and Khoo[1]: Λ_β and $v_{\beta\text{-}rms}$. Λ_β is defined as the region where the variation of $V_{r\text{-rms}}$ remains linear; $v_{\beta\text{-}rms}$ is taken to be the velocity denoting the magnitude of $V_{r\text{-rms}}$ at the distance of

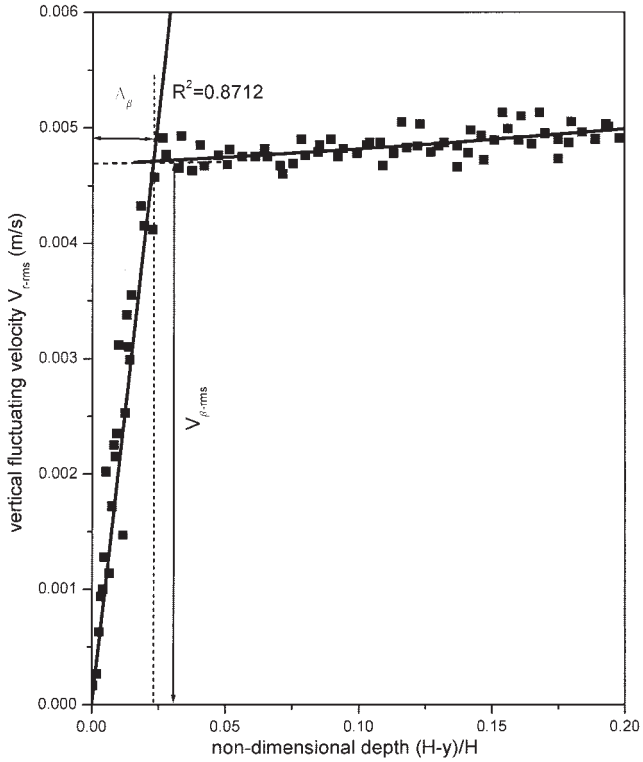

Figure 5. Variation of $V_{r\text{-rms}}$ with nondimensional depth.

Λ_β beneath the interface. After obtaining the value of β_{rms}, a second nonlinear fit can be carried outside the linear region. The extrapolated interception of the linear fit with the nonlinear curve fit is obtained and chosen to determine the value of Λ_β and $v_{\beta\text{-}rms}$ (see Figure 5).

Figure 6 shows the variation of β_{rms} with the nominal wind speeds for all of the flow conditions studied. The results of Law and Khoo[1] for only wind-induced flow conditions are also included. It can be seen that this selected parameter generally increased with the wind speed, clearly indicating that the near-surface turbulence intensity expressed in terms of β_{rms} in the linear region is dependent on the imposed wind speed from above and the water flow velocity from beneath. With respect to a comparison of the different β_{rms} values under the same water flow rate, it can be seen that turbulence generated in cocurrent flow (that is, the wind above and water below the interface are imposed in the same direction) is deemed to have the largest turbulence intensity in the vicinity of the interface region, whereas turbulence generated in countercurrent has the smallest turbulence intensity in that region. Under the lower water flow rate conditions (3.2 and 6.3 mL/s), Figure 6 indicates that the near-surface turbulence is primarily determined by the wind speed induced from above. Finally, it may be mentioned regarding the comparison of the present results to Law and Khoo[1] for the wind only, that the deviations occur primarily in the low wind speed range, usually associated with lower flow velocities and larger measurement errors or uncertainties; the differences are limited to about 20%.

Mass-transfer velocity

Figure 7 shows the mass-transfer velocity in the studied flow conditions. From this figure, it can be seen that the mass-

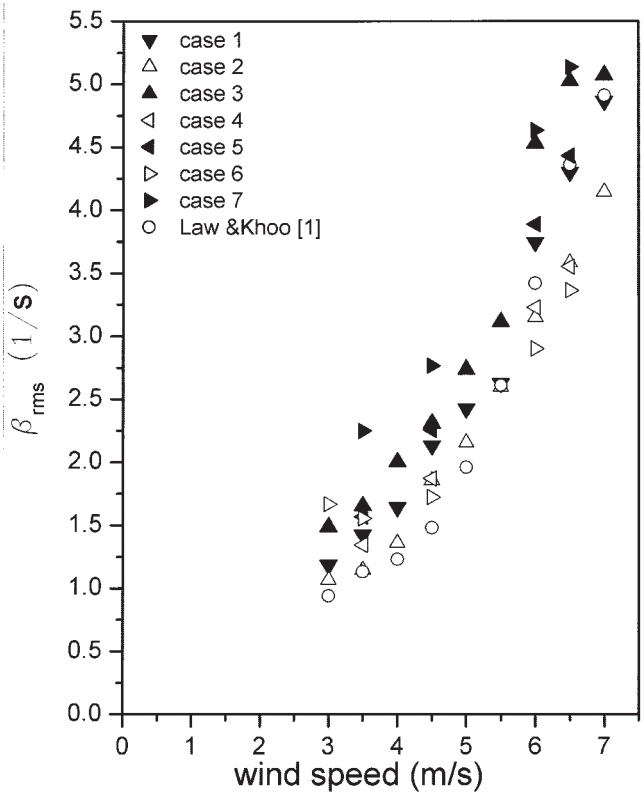

Figure 6. Variation of β_{rms} with nominal wind speed for Cases 1–7 (see Table 1).

transfer velocity generally increases with wind speed. This again demonstrates the general trend between turbulence intensity with mass-transfer velocity. The mass-transfer velocity in Figure 7a shows a fairly linear behavior passing through the origin for the case where only wind speed is imposed. A closer scrutiny reveals that for the case of the same direction (Figure 7b), K_L assumes a value perceptibly higher than the linear profile as obtained in Figure 7a. On the other hand, K_L for the case of the opposite direction (Figure 7c) takes on quantities clearly below the linear region depicted in Figure 7a. This observation is not too surprising, as deduced from Figure 6, if one presupposed that the mass transfer is directly proportional to β_{rms}. A careful examination of Figures 7a, 7b, and 7c suggests that in a comparison with the gas evasion results, the mass-transfer velocity obtained by the gas absorption experiment seems to assume a larger quantity and the difference tends to increase as the wind speed increases. Overall, the β_{rms} data of Figure 6 and the K_L data of Figure 7 depict the same trend as the wind speed increases.

For direct comparison with the previous results of Law and Khoo[1] and Jahne and Munnich[19] carried out in a similar circular wind-wave channel, the mass-transfer velocity is depicted together with Sc as $K_L Sc^{0.5}$ for the ordinate axis and plotted vs. the wind speed on the abscissa axis. The use of $K_L Sc^{0.5}$ assumes a relationship of K_L to the diffusion coefficient of the gas in water, used by many others, and also to account for the different tracer gas used in the different experiments. It is noted that in Law and Khoo,[1] CO_2 was used at a water temperature of about 27°C (Sc ≈ 420). In Jahne and Munnich's work, CO_2 was used at a water temperature of about 20°C (Sc ≈ 600), whereas in this work, O_2 was used at a water temperature of about 22°C (Sc ≈ 532). Figure 8 shows reasonably good

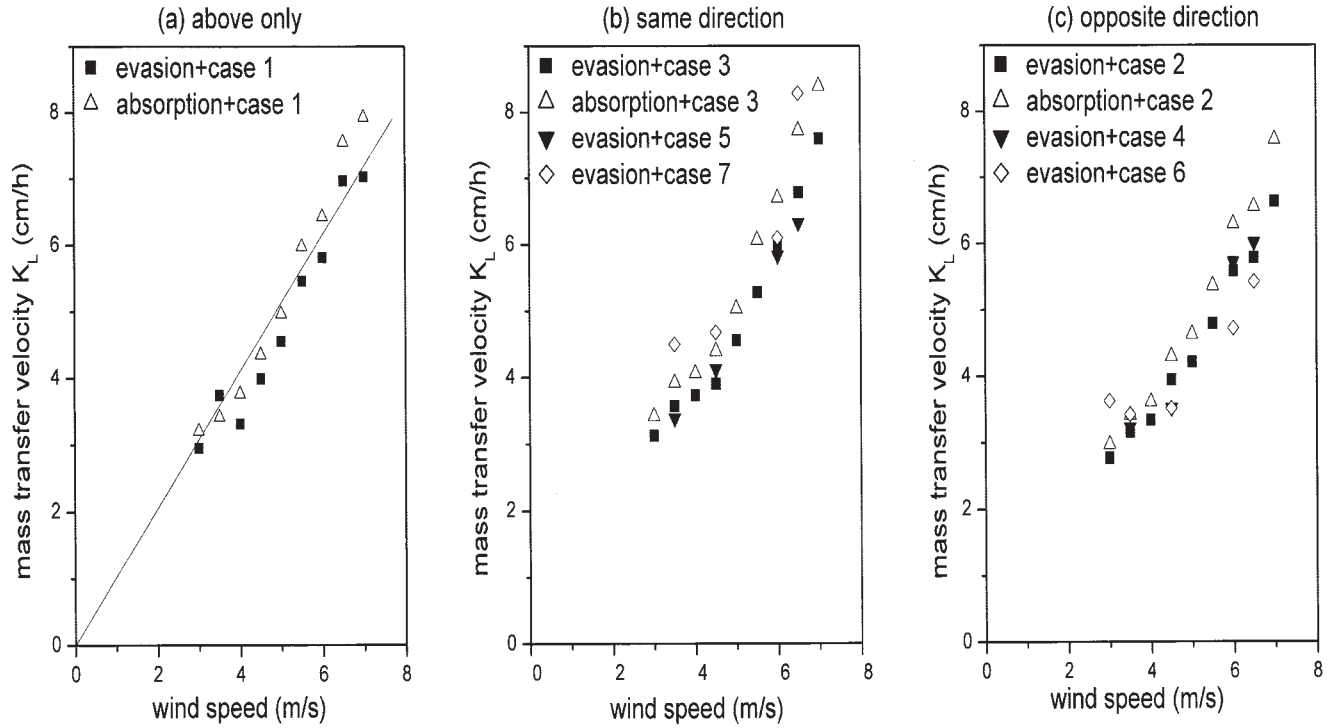

Figure 7. Mass-transfer velocity vs. wind speed.

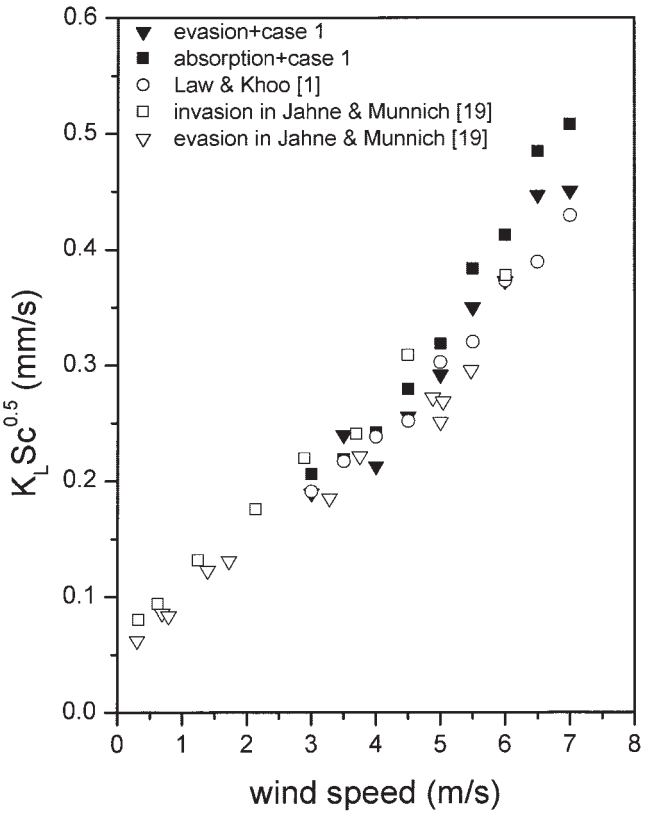

Figure 8. Comparison of the mass-transfer velocity varying with nominal wind speed.

concurrence in value and trend with Law and Khoo[1] and Jahne and Munnich.[19]

Discussion

Correlation of the mass-transfer coefficient and near-surface turbulence parameters was previously investigated by such researchers as McCready et al.,[8] Khoo and Sonin,[20] and Tamburrino and Gulliver.[6] The relation can be expressed as

$$K_L^+ \equiv \frac{K_L}{v_{\beta-rms}} = f\left[\left(\frac{\beta_{rms}\nu}{v_{\beta-rms}^2}\right)^{0.5}\right] \mathrm{Sc}^{-0.5}. \tag{10}$$

Here $K_L^+ \equiv K_L/v_{\beta\text{-}rms}$ is the nondimensional mass-transfer velocity, $\beta_{rms}^+ \equiv \beta_{rms}\nu/v_{\beta\text{-}rms}^2$ is the nondimensional form of β_{rms}, and $f(\cdot)$ indicates a functional relationship. The exponent for Sc is governed by the surface conditions. McKenna and McGillis[4] investigated the role of surfactant in gas–water mass transfer and presented an expression for the Schmidt number exponent as $n = (2/3) - [(1/6)e^{-\zeta/2}]$, where ζ is defined as stress ratio. In this work, the mass-transfer experiment is done in the condition of a clean surface. Under such conditions the stress ratio is zero, so the exponent of Sc is set to 0.5.

It is noted that the nondimensional parameter β_{rms}^+ encompasses all three of the parameters (β_{rms}, Λ_β, and $v_{\beta\text{-}rms}$) that define the hydrodynamics characteristics in the vicinity of the interface region. Even though Λ_β does not appear explicitly in the definition of this nondimensional parameter, its influence is implicitly represented by the definition of β_{rms}. For sparingly soluble gases (such as CO_2 and O_2), the concentration boundary layer next to the interface is very thin. Thus, the hydrodynamics characteristics in the immediate vicinity of the interface region are deemed to be crucial for the mass-transfer process, and the other important issue is that such parameters exist irrespective of the turbulence generation mechanism. The above-mentioned features found in the mass-transfer correlation model based on β in Law and Khoo[1] look promising and possess the potential to be further developed into a robust model that is applicable to different flows.

Figure 9 shows the plot of $K_L^+ \mathrm{Sc}^{0.5}$ vs. $(\beta_{rms}^+)^{0.5}$ for all the studied flow conditions based on both gas evasion and absorption measurements in our experiments. The result of Law and Khoo[1] is also included. In the work of Law and Khoo,[1] turbulence is imposed through two distinct methods: a wind-induced shear turbulence from above and, separately, a confined-jet turbulence induced from beneath in a half-filled cylinder with water. Various water–glycerol mixtures, using widely ranging combinations of liquid and carbon dioxide gas, were tested at different temperatures. A combination of their works where β_{rms} values were explicitly measured with the present data will help to build a more universal correlation. It can be observed that a linear behavior (slope = 0.20 with $R^2 = 0.981$) can still be realized for all of the presented flow conditions. From Figure 9, a general relation can be proposed to correlate the mass-transfer velocity with the near-surface turbulence parameters:

$$K_L^+ \mathrm{Sc}^{0.5} = 0.2(\beta_{rms}^+)^{0.5}. \tag{11}$$

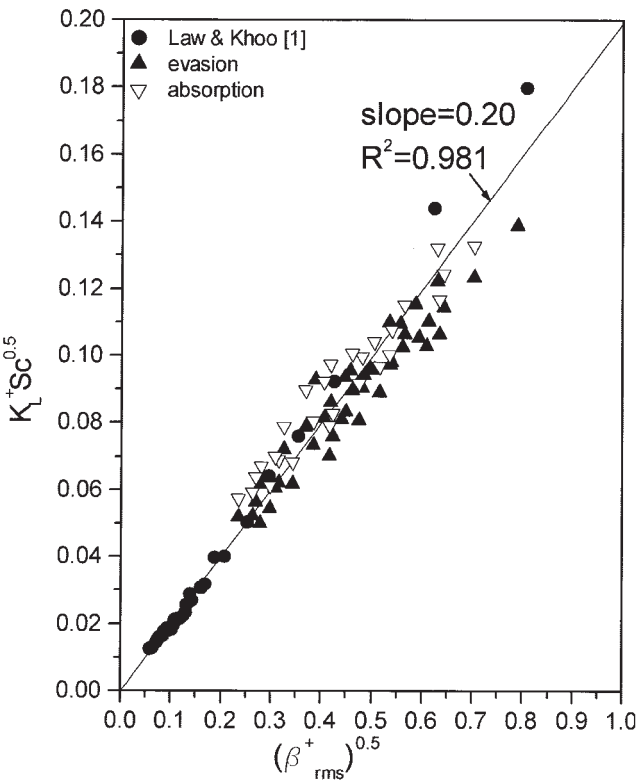

Figure 9. $K_L^+ Sc^{0.5}$ vs. $(\beta_{rms}^+)^{0.5}$ for all the tested flow conditions.

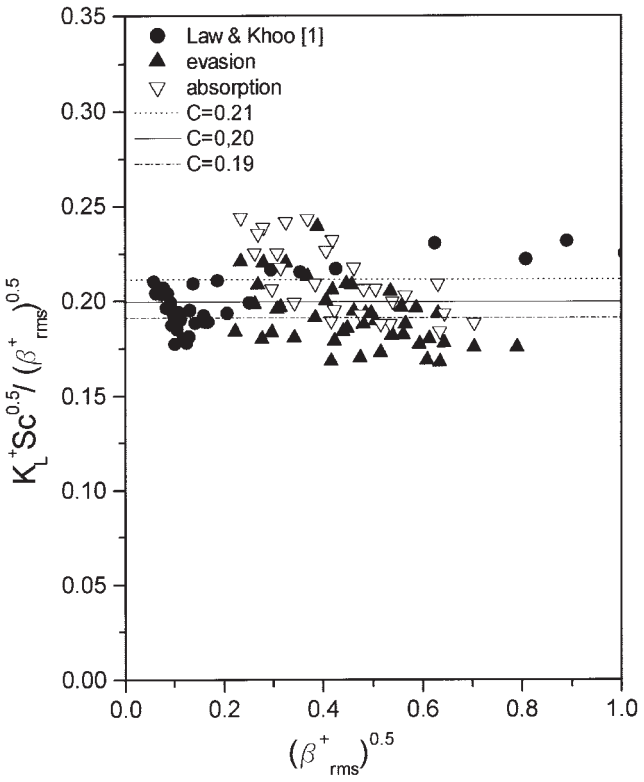

Figure 10. $K_L^+Sc^{0.5}/(\beta^+_{rms})^{0.5}$ vs. $(\beta^+_{rms})^{0.5}$ for all the tested flow conditions.

Figure 10 shows a replot of all the results expressed in terms of $K_L^+Sc^{0.5}/(\beta^+_{rms})^{0.5}$ vs. $(\beta^+_{rms})^{0.5}$. For only the gas absorption experiments in our measurements, the data present a mean value of 0.21, whereas for the gas evasion experiments only, a mean value is obtained as 0.19. For all of the presented data points including the data from Law and Khoo,[1] the overall mean quantity is 0.20. The difference noted for the different mean quantities is $<10\%$ and broadly suggests the correlation obtained is valid for both gas absorption and evasion, despite the larger experimental uncertainty associated with the gas absorption measurement.

A very recent work on direct numerical simulation (DNS) of a vertical rotating open-channel flow with heat transfer at the free surface can be found in Li et al.[21] Li et al. used the correlation relation of Law and Khoo,[1] reexpressed as

$$\mathrm{Nu}\,\mathrm{Pr}^{0.5} = 0.22\left(\mathrm{Re}_\tau \left|\frac{\partial v'_{rms}}{\partial y}\right|_{y=1}\right)^{0.5}. \tag{12}$$

Their DNS results concur very well with Eq. 12 in terms of trend as the rotational speed increases as depicted in their Figure 7. The magnitude also agrees reasonably well except that the computed results indicated a slight underprediction. In fact if the coefficient in Eq. 12 is reduced to say 0.20 as proposed in Eq. 11, the concurrence would have been even better. The most important observation is that in Li et al., the turbulence near the free surface is generated by rotation and yet the scalar transport in terms of heat transfer across the turbulent air–water interface behaves remarkably as determined by Eq. 11. This further supports the possible universality of Eq. 11.

Comparison with other similar models

In recent years, the designation "surface divergence model" has been given to the model for a quantitative description of the gas–liquid interface given nominally by the parameter $(\nabla_h \cdot \mathbf{V})$, where ∇_h is the horizontal two-dimensional divergence operator and $\mathbf{V}$ is the velocity fluctuation vector. It is clear that $(\nabla_h \cdot \mathbf{V})$ is equivalent to β as first shown by Tamburrino,[22] and also noted in Tamburrino and Gulliver[6] and McKenna and McGillis.[4] To consider the possible large deformation of the interface, Banerjee et al.[23] modified the mentioned equivalence by additional terms relating to the curvature of the fluctuating interface as opposed to a flat interface (see Eq. 16 below). Nevertheless, in most experiments, if the fluctuating amplitude of the interface is kept deliberately limited and in an absence of wave breaking, the relationship between the gradient of vertical velocity taken with respect to the interface and defined as β here is still closely linked by to the negative two-dimensional divergence of the free surface.

A detailed experimental work was carried out by Tamburrino and Gulliver[6] in a fully developed straight section channel flow, where turbulence is generated from beneath the interface (in the absence of any wind-imposed shear from above). Tamburrino and Gulliver emphasized and used the maximum value of the β frequency spectrum instead of the mean value of β in the near-surface region. Together with the mass-transfer measurements from Gulliver and Halverson[24] and Lau,[25] they proposed a correlation of the form

$$K^+\sqrt{\mathrm{Sc}} = 0.24\sqrt{S^+_{\beta\,\max}}. \tag{13}$$

However, from an estimate of the various relevant tabulated quantities found from their Tables 1 and 3, such as $\bar{\beta}^{+2}$, $\bar{\beta}^2$, and $S^+_{\beta\,\max}$, we can obtain a reworked relationship as

$$\frac{K_L^+\mathrm{Sc}^{0.5}}{(\beta^+_{rms})^{0.5}} \approx 0.151. \tag{14}$$

This relationship and the experimental measurements of Tamburrino and Gulliver[6] are also plotted in Figure 11 for comparison, which indicates fair agreement with the present results. This suggests the critical importance of $S^+_{\beta\,\max}$ in the correlation for the mass transfer across the gas–water interface as argued and proposed by Tamburrino and Gulliver[6] can be viewed alternatively in terms of β^+_{rms}. It may be mentioned that the deviation mainly lies in the lower β value region, which corresponds to the low turbulence intensity region. In taking account of the measurement uncertainty and the limited experimental conditions carried out in Tamburrino and Gulliver,[6] the difference in the coefficients of Eqs. 11 and 14 is deemed to be acceptable.

McKenna and McGillis[4] used an innovative DPIV technique to measure the surface divergence under an oscillating grid-stirred turbulence. Their work is focused on the role of surfactant on the scalar transport across the gas–liquid interface and proposes a relationship in the form as

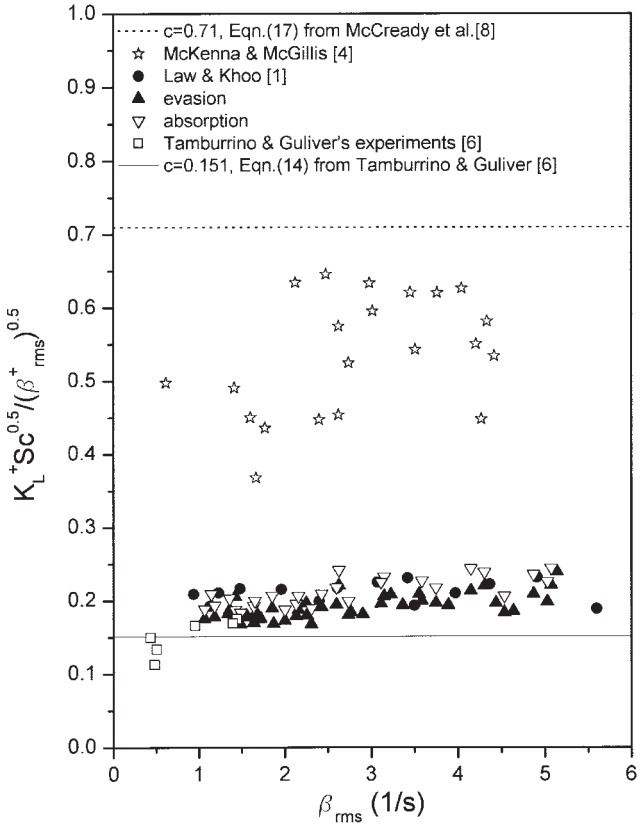

Figure 11. Comparison of various works.

$$K^+ = \frac{k}{aL} = \frac{1}{2}\,\mathrm{Re}_a^{-1/2}\mathrm{Sc}^{-n} \qquad n = \frac{2}{3} - \frac{1}{6}\,e^{-\varphi/2} \tag{15}$$

where $a = (\nabla_h \cdot \mathbf{V})$ is defined as surface divergence, $\mathrm{Re}_a = aL^2/\nu$, and the Schmidt number exponent n is governed by surface conditions. Under a clean surface condition, $n = 0.5$. A macrolength scale L is used to determine a dimensionless quantity. For direct comparison with the results from Law and Khoo[1] and the present work, the dimensional parameter β (or a) is used on the abscissa axis and plotted in Figure 11. The general trend of the present results fit well with the measurements of McKenna and McGillis, whereas an obvious difference exists in term of the magnitude. Their results show a significant scattered pattern. In McKenna's thesis,[26] it was pointed out that there were several contributory factors to the experimental uncertainty for their work. One such factor arose from the uncertainty in the DPIV measurement of roughly 10–30%. The other part is the limitation of the measurement determined by the spatial resolution. Brumley and Jirka[27] derived some theoretical results and suggested that the smallest scales contribute the most to the surface divergence, whereas the finite spatial resolution of around 6 mm in the work by McKenna and McGillis omits the contributions of such smaller scales, which can result in the underestimation of the flow dynamics parameters. This would be an essentially consistent shift over all the measurements, rather than a random measurement uncertainty. This part of uncertainty is hard to estimate, but the magnitude is reckoned to be not negligible. We can only surmise qualitatively that the difference observed between Eqs. 11 and 15 is largely attributed to the dramatically different measurement techniques for β (or a).

Banerjee et al.[23] in their DNS study of the surface divergence models for scalar exchange between turbulent streams suggested a relationship that can be reexpressed as

$$\frac{K\mathrm{Sc}^{0.5}}{u} \approx \frac{C}{\mathrm{Re}_t^{0.5}}\left[\left(\frac{\partial u'}{\partial x} + \frac{\partial v'}{\partial y} - 2w'\nabla\cdot n\right)^2\right]^{1/4}. \tag{16}$$

Here the term in parentheses embedded within the square brackets on the right-hand side is the surface divergence, taking into consideration the curvature of the deforming surface, and C is a coefficient. Their DNS calculations showed that the said surface divergence term with the dilation contribution is numerically the same as another form obtained based on the Hunt–Graham[28] blocking theory (their Figure 8), such that $C \approx 0.20$ for Eq. 16 appears to concur rather well with the experimental data of Komori et al.[29] for an unsheared interface of an open channel flow (see their Table 2 for comparison of the measured mass-transfer coefficient from Komori et al. and their prediction). For the DNS of the sheared turbulent air and water streams, from the rather limited data set, Banerjee et al.[23] obtained a higher coefficient of $C \approx 0.35$ (for the lower Sc of 1.0–1.2) and $C \approx 0.45$ (for the higher Sc up to about 200). It is unfortunate that the quantitative values of equivalent β^+_{rms} (or dimensional β) are not provided explicitly and cannot be easily deduced to be reflected directly in either Figure 10 or Figure 11 for more detailed comparison and evaluation. Nevertheless, despite the differences in the coefficient in Eqs. 16 and 11, which can be attributed to how the surface divergence is defined and related to β, the trend is unmistakenly similar and valid for a varied range of flow conditions irrespective of how the surface turbulence is generated.

Finally, as already discussed somewhat at length in Law and Khoo,[1] McCready et al.[8] performed a computer simulation of liquid flow beneath a flat mobile interface next to the gaseous medium. As indicated by the authors that there is not enough experimental information to determine $\beta(z, t)$ completely, they just assumed that the spatial variation of the velocity field was represented by a single harmonic of the form as

$$\beta(z, t) = \sqrt{2}\beta(t)\cos(2\pi z/\lambda_z) \qquad \text{and} \qquad v = \beta(z, t)y \tag{17}$$

where $\beta(t)$ is a random function of time and z is the transverse coordinate. The transverse wavelength λ_z was taken to be 100 (made dimensionless with interfacial friction velocity and kinematic viscosity) for most of the calculations so as to be consistent with the measured behavior near a solid boundary. Although these and several other assumptions were used in their derivation, McCready et al. obtained a relation linking the scalar transport across the interface to β as

$$K_L^+\mathrm{Sc}^{0.5} = 0.71(\beta^+_{rms})^{0.5}. \tag{18}$$

This relation is plotted in Figure 11 for comparison. It is appropriate to note the characteristic velocity used in the nondimensionalization appeared on both sides of Eq. 18 (and/or Eq. 11 and others) and can be cancelled out, thus leaving the functional completely unaffected. McCready et al.[8] used a

different characteristic velocity scale for their nondimensionalization. It is clear that Eq. 18 is consonant with Eq. 11 except for the magnitude of the coefficient, which can be easily attributed to the assumptions made in McCready et al.

Overall, from the discussions above, the coefficient still obtained as $C \sim O(1.0)$ for the vastly different works may portend well and point toward the possibility of a universal constant or a constant with some limited variability. Further work is certainly necessary to establish whether the variation in C is inherent or otherwise. Still, having established β or the surface divergence as the key or primary parameter responsible for the scalar transport across the turbulent gas–liquid interface, the next step forward—as for most engineering applications—lies in how to affect the flow conditions to increase/decrease the said key parameter for enhancement/moderation of the associated scalar transport.

Conclusion

It is increasingly clear that use of the bulk turbulence cannot provide a unique relationship between the turbulence hydrodynamics and the scalar transfer velocity, and the flow hydrodynamics in the immediate vicinity of the interface—like the vertical velocity gradient (β or the surface divergence)—plays an important role in determining the transport process, which is fairly independent of the means of turbulence generation. Based on the improved measurement method provided in this work, quantification of the vertical velocity with respect to the fluctuating interface and evaluation of the associated velocity gradient in the vicinity of the interface were carried out. The critical parameter β was obtained under vastly different and distinct flow conditions. These mentioned distinct flow conditions are turbulence induced by wind shear from above, turbulence generated and diffused to the free surface from beneath the interface, and a combination of simultaneously contributing conditions from above and beneath the gas–liquid interface. All of them can be regarded as the simplifications of all the other turbulence generation methods. Results from the mass-transfer experiments suggest a possible general relationship of the form

$$\frac{K_L}{(\beta_{rms}\nu)^{0.5}}\,\mathrm{Sc}^{0.5} = C \approx 0.20. \tag{19}$$

This expression correlates the interfacial hydrodynamics parameter and the mass-transfer velocity. The proposed correlation has found good concurrence at least in terms of trends with other reported works where turbulence is generated differently such as in grid-stirred turbulence, a submerged moving bed plume, and flow down an induced plane. The mentioned concurrence is true with $C \sim O(1.0)$.

Notation

A = area of the interface, m^2
C = concentration of the gas species in liquid, mol/m^3
C_i = initial concentration of gas species in liquid, mol/m^3
C_f = final concentration of gas species in liquid after time t_f, mol/m^3
C_s = gas species concentration at the water surface, mol/m^3
C_b = gas species concentration in bulk region of the liquid side, mol/m^3
D = diffusion coefficient, m^2/s
F = transport of gaseous species across an interface per unit area, $mol \cdot m^{-2} \cdot s^{-1}$
K_L = liquid-side mass-transfer velocity, m/s
L = macrolength scale, m
R = distance from the center of the rotation to the center of the water channel, m
Sc = Schmidt number
u^* = interfacial friction velocity, m/s
U_{mean} = mean flow velocity in the horizontal direction, m/s
v = vertical velocity component, m/s
v_i = interface vertical velocity, m/s
v_r = vertical velocity with respect to the interface, m/s
V_β = velocity scale where $v_{r\text{-rms}}$ departs from the linear behavior, m/s
V_w = the volume of water in the system, m^3
T = temperature of the water, °C

Greek letters

δ = thickness of the mass boundary layer, m
β = vertical velocity gradient at the interface, 1/s
τ = surface renewal time, s
ε = rate of turbulence dissipation, m^2/s^3
ω = rotation speed of the rotor driving the paddles, rad/s
ρ = density, kg/m^3
ν = liquid kinematic viscosity, m^2/s
Λ_β = distance from the interface where the variation of $v_{r\text{-rms}}$ remains linear, m

Subscript

rms = root mean square

Literature Cited

1. Law CNS, Khoo BC. Transport across a turbulent gas–water interface. *AIChE J.* 2002;48:1856-1868.
2. Molder E, Tenno T, Mashirin A. The effect of surfactants on oxygen mass-transfer through the gas–water interface. *Environ Sci Pollut Res.* 2002;(Special Issue 1):39-42.
3. Vasconcelos JMT, Rodrigues JML, Orvalho SCP, Alves SS, Mendes RL, Reis A. Effect of contaminants on mass transfer coefficients in bubble column and airlift contactors. *Chem Eng Sci.* 2003;:31-40.
4. McKenna SP, McGillis WR.The role of free-surface turbulence and surfactants in gas–water gas transfer. *Int J Heat Mass Transfer.* 2004; 47:539-553.
5. Theofanous TG. Conceptual models of gas exchange. In: Brutsaert W, Jirka GH, eds. *Gas Transfer at Water Surfaces*. Dordrecht, Thye Netherlands: D. Reidel; 1984:271-281.
6. Tamburrino A, Gulliver JS. Free surface turbulence and mass transfer in a channel flow. *AIChE J.* 2002;48:2732-2743.
7. Hanratty TJ. Effect of gas flow on physical adsorption. In: Wilhelm SC, Gulliver JS, eds. *Air–Water Mass Transfer*. New York: ASCE; 1991:10-33.
8. McCready MJ, Vassihadou E, Hanratty TJ. Computer simulation of turbulent mass transfer at a mobile interface. *AIChE J.* 1986;32:1108-1115.
9. Hassan YA, Okamoto K, Philip OG. Investigation of the interaction between a fluid flow and the fluid's free surface using particle image velocimetry. Proceedings of the Ninth International Symposium on Transport Phenomena in Thermal-Fluids Engineering (ISTP-9), Singapore; 1996;566-574.
10. Peirson WL. Measurement of surface velocities and shears at a wavy gas–water interface using particle image velocimetry. *Exp Fluids.* 1997;23:427-437.
11. Law CNS, Khoo BC, Chew TC. Turbulence structure in the immediate vicinity of the shear-free air–water interface induced by a deeply submerged jet. *Exp Fluids.* 1999;27:321-331.
12. Jahne B, Wierzimok D. Measurement of wave-induced turbulent flow structures using digital image sequence analysis. In: Wilhelm SC, Gulliver JS, eds. *Air–Water Mass Transfer*. New York: ASCE; 1991: 200-209.
13. Lorencez C, Nasr-Esfahany M, Kawaji M. Turbulence structure and

prediction of interfacial heat and mass transfer in wavy-stratified flow. *AIChE J.* 1997;43:1426-1435.
14. Baumann KH, Muhlfriedel K. Mass transfer and concentration profiles near phase boundaries. *Int J Therm Sci.* 2001;40:425-436.
15. Lin HJ, Perlin M. Improved methods for thin surface boundary layer investigations. *Exp Fluids.* 1998;25:431-444.
16. Munsterer T, Jahne B. LIF measurements of concentration profiles in the aqueous mass boundary layer. *Exp Fluids.* 1998;25:190-196.
17. Ridler TW, Calvard S. Picture thresholding using an iterative selection method. *IEEE Trans Syst Man Cybern.* 1978;8:630-632.
18. Katznelson R. DQM standard operation procedure (SOP) 9.2.1.2(V3); 2004. http://www.swrcb.ca.gov/nps/docs/cwtguidance/9212sop.pdf.
19. Jahne B, Munnich KO. Measurements of gas exchange and momentum transfer in a circular wind-wave tunnel. *Tellus.* 1979;31:321-329.
20. Khoo BC, Sonin AA. Scalar rate correlation at a turbulent water free surface: A two-regime correlation for high Schmidt number. *Int J Heat Mass Transfer.* 1992;35:2233-2244.
21. Li BY, Liu NS, Lu XY. Direct numerical simulation of vertical rotating turbulent open-channel flow with heat transfer. *Commun Comput Phys.* 2006;1:336-361.
22. Tamburrino A. *Free-Surface Kinematics: Measurement and Relation to the Mass Transfer Coefficient in Open Channel Flow*. PhD Thesis. University of Minnesota (Twin Cities), MN; 1994.
23. Banerjee S, Lakehal D, Fulgosi M. Surface divergence models for scalar exchange between turbulent streams. *Int J Multiphase Flow.* 2004;30:963-977.
24. Gulliver JS, Halverson MJ. Air–water gas transfer in open channels. *Water Resour Res.* 1989;25:1783-1793.
25. Lau YL. An experimental investigation of reaeration in open channel flow. *Prog Water Technol.* 1975;7(3/4):519-530.
26. Mckenna SP. *Free-Surface Turbulence and Air–Water Gas Exchange*. PhD Thesis. Cambridge, MA: MIT; 2000.
27. Brumley BH, Jirka GH. Air–water transfer of slightly soluble gases: Turbulence. Interfacial processes and conceptual models. *Physicochem Hydrodyn.* 1988;10:295-319.
28. Hunt JCR, Graham JMR. Free stream turbulence near plane boundaries. *J Fluid Mech.* 1978;84:209-235.
29. Komori S, Murakami Y, Ueda H. The relationship between surface renewal and bursting motions in an open channel flow. *J Fluid Mech.* 1989;203:103-123.

Manuscript received Mar. 23, 2006, and revision received July 11, 2006.